



# Biradical-Featured Stable Organic-Small-Molecule Photothermal Materials for Highly Efficient Solar-Driven Water Evaporation

Guanyu Chen, Jiangman Sun, Qian Peng, Qi Sun, Guan Wang, Yuanjing Cai, Xinggui Gu,\* Zhigang Shuai, and Ben Zhong Tang\*

With recent progress in photothermal materials, organic small molecules featured with flexibility, diverse structures, and tunable properties exhibit unique advantages but have been rarely applied in solar-driven water evaporation owing to limited sunlight absorption resulting in low solar–thermal conversion. Herein, a stable croconium derivative, named CR-TPE-T, is designed to exhibit the unique biradical property and strong  $\pi$ – $\pi$  stacking in the solid state, which facilitate not only a broad absorption spectrum from 300 to 1600 nm for effective sunlight harvesting, but also highly efficient photothermal conversion by boosting nonradiative decay. The photothermal efficiency is evaluated to be 72.7% under 808 nm laser irradiation. Based on this, an interfacial-heating evaporation system based on CR-TPE-T is established successfully, using which a high solar-energy-to-vapor efficiency of 87.2% and water evaporation rate of 1.272 kg m<sup>-2</sup> h<sup>-1</sup> under 1 sun irradiation are obtained, thus making an important step toward the application of organic-small-molecule photothermal materials in solar energy utilization.

conversion of solar energy,<sup>[2]</sup> and has been employed to address the serious water shortage based on solar-driven water evaporation.<sup>[3]</sup> Emerging concept of localized interfacial heating for construction of water evaporation system has been put forward to effectively improve the conversion efficiency of solar energy,<sup>[4]</sup> which is highly dependent on exploration of efficient photothermal materials with broad solar absorption, chemical/thermal/photostability, and highly efficient photothermal conversion.<sup>[3a,5]</sup> So far, various energy-efficient photothermal materials have been developed for conversion of solar energy to heat, while mainly focused on metal-based inorganic materials,<sup>[6,7]</sup> carbon-based materials,<sup>[8,9]</sup> and conjugated polymers.<sup>[1c,10,11]</sup> Actually, photothermal materials based on organic small molecules, bearing their unique superiorities

Solar energy has been considered as clean and renewable energy and its highly efficient conversion has been extensively pursued through photochemical, photovoltaic, and photothermal processes, with the aim to solve the scarcity of energy resources in an environmentally friendly manner.<sup>[1]</sup> Among them, solar–thermal conversion has recently been attracting expanding interest due to the direct and high-efficiency

in flexibility, diverse structures, and fine-tuned properties, have recently been the subject of increasing interest for biomedical applications by converting near-infrared (NIR) light into heat via nonradiative decay.<sup>[12,13]</sup> However, they have somehow missed research attention in solar-driven water evaporation. This is mainly due to the concern that photobleaching and limited sunlight absorption will lead to the low-efficiency solar–thermal

G. Chen, Prof. J. Sun, Dr. G. Wang, Prof. Y. Cai, Prof. X. Gu  
Beijing Advanced Innovation Center for Soft Matter Science and Engineering  
College of Materials Science and Engineering  
State Key Laboratory of Chemical Resource Engineering  
Beijing University of Chemical Technology  
Beijing 100029, China  
E-mail: guxinggui@mail.buct.edu.cn

Prof. Q. Peng  
Key Laboratory of Organic Solids  
Beijing National Laboratory for Molecular Sciences (BNLMS)  
Institute of Chemistry  
Chinese Academy of Sciences  
Beijing 100080, China

Q. Sun, Prof. Z. Shuai  
Key Laboratory of Organic Optoelectronics and Molecular Engineering  
Department of Chemistry  
Tsinghua University  
Beijing 100084, China

Prof. B. Z. Tang  
Department of Chemistry  
Hong Kong Branch of Chinese National Engineering Research Center for Tissue Restoration and Reconstruction  
Institute for Advanced Study  
The Hong Kong University of Science and Technology  
Clear Water Bay, Kowloon, Hong Kong, China  
E-mail: tangbenz@ust.hk

Prof. B. Z. Tang  
Center for Aggregation-Induced Emission  
SCUT-HKUST Joint Research Institute  
State Key Laboratory of Luminescent Materials and Devices  
South China University of Technology  
Guangzhou 510640, China

The ORCID identification number(s) for the author(s) of this article can be found under <https://doi.org/10.1002/adma.201908537>.

DOI: 10.1002/adma.201908537

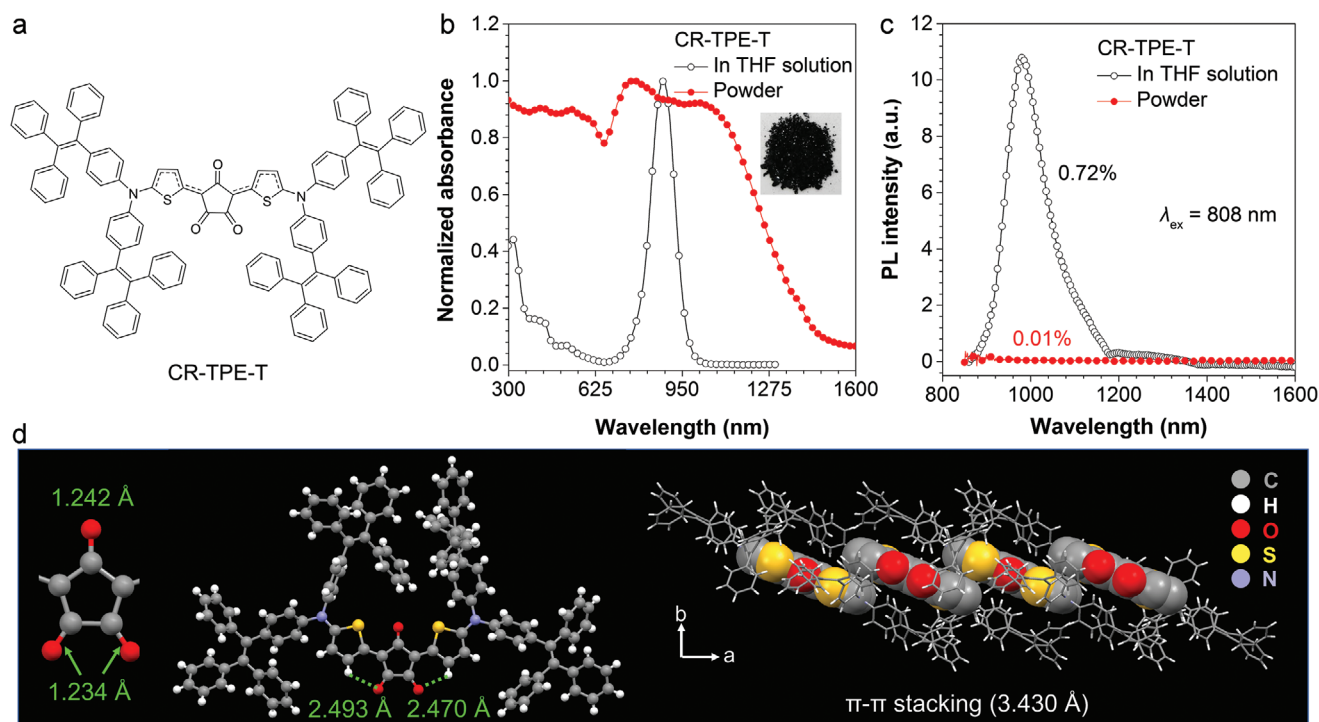


**Figure 1.** a) Chemical structure of CR-TPE-T. b,c) The absorption and photoluminescent (PL) spectra of CR-TPE-T in THF solution and powder. Inset shows the photo of CR-TPE-T powder taken under daylight. Excitation wavelength ( $\lambda_{ex}$ ) is 808 nm. d) Single-crystal X-ray analysis of CR-TPE-T: the bond lengths of carbonyl groups in croconic core, the intramolecular interactions between thiophene and croconic core, and the intermolecular  $\pi$ - $\pi$  stacking of CR-TPE-T.

conversion.<sup>[14–16]</sup> Thus, development of stable organic-small-molecule photothermal materials with broad solar absorption is the key to enable highly efficient solar energy conversion, which is fascinating but challenging.

Organic-small-molecule croconium dyes (CRs),<sup>[17–19]</sup> with proposed resonance electronic structure between mesoionic and biradical forms,<sup>[20]</sup> have been reported to exhibit superior chemical/thermal/photostability and photothermal effects compared to conventional NIR counterparts,<sup>[12–15]</sup> thus becoming potential candidates for solar-driven water evaporation. Up to now, most of the CRs have exhibited intense but narrow absorption at about 800 nm, making them difficult to harvest sunlight sufficiently. Therefore, reasonable molecular design is urgently required to endow CRs with effective solar absorption. Generally, organic conjugated molecules with strong electron donor–acceptor coplanar skeleton present redshifted absorption by effective electron delocalization.<sup>[21]</sup> Such bathochromic shift of the absorption will be largely promoted when radicals are generated in the conjugated structure.<sup>[22]</sup> On the other hand, the  $\pi$ - $\pi$  stacking formed in the aggregates of organic conjugated molecules could further extend their absorption spectrum. More interestingly, the resultant small energy gap could boost nonradiative decay for generating heat according to the energy-gap law.<sup>[23]</sup> Therefore, the introduction of radicals and strong  $\pi$ - $\pi$  stacking based on a strong electron donor–acceptor coplanar structure could achieve the extended solar absorption and effectively enable the photothermal conversion for CRs upon aggregation, which will be an effective way to efficiently convert solar energy to heat for water evaporation.

With this in mind, a high-performance and stable CR-based organic-small-molecule photothermal material, named as CR-TPE-T (Figure 1a), was well designed and readily synthesized. It exhibited a broad absorption spectrum from 300 to 1600 nm in the solid state, effectively facilitating the absorption of sunlight. As expected, the open-shell biradical character of CR-TPE-T was observed and further increased upon aggregation, and the strong  $\pi$ - $\pi$  stacking was clearly revealed in the crystal of CR-TPE-T by single-crystal X-ray analysis. Due to the low energy gap of 0.75 eV, the nonradiative decay was largely boosted based on the energy-gap law, which greatly enhances the solar-thermal conversion for CR-TPE-T in the solid state. Indeed, the photothermal efficiency was evaluated to be larger than 72.7% upon 808 nm laser irradiation, and the high temperature could be achieved upon irradiation of 1 sunlight. Based on these, a composite CR-TPE-T-loading PU foam was fabricated to establish an interfacial-heating evaporation system. The solar energy-to-vapor efficiency and water evaporation rate were evaluated up to 87.2% and 1.272 kg m<sup>-2</sup> h<sup>-1</sup> under 1 sunlight, respectively, which are comparable to those of reported materials.<sup>[4–11,24]</sup> This work unveils the huge potential of organic-small-molecule photothermal materials in highly efficient utilization of solar energy.

First, CR-TPE-T was simply synthesized by undergoing the route depicted in Scheme S1, Supporting Information, with a yield of 52%. All the structures of CR-TPE-T and its intermediates were carefully characterized by NMR and high-resolution mass spectrometry (Figures S1–S5, Supporting Information). Within the molecular structure of CR-TPE-T (Figure 1a), two

electron-donating tetraphenylethylene (TPE) units were symmetrically decorated on thiophene (T)-substituted croconium. Such structural characteristic for CRs has been demonstrated to possess excellent high chemical/thermal/photostability before.<sup>[17b]</sup> Then, the photophysical properties of CR-TPE-T in both solution and the solid states were investigated. As shown in Figure 1b and Figure S6a, Supporting Information, it absorbs intensely in THF solution with the high molar absorption coefficient ( $\epsilon$ ) of  $1.84 \times 10^5 \text{ L mol}^{-1} \text{ cm}^{-1}$  at 880 nm. By comparison to traditional CRs,<sup>[17,18]</sup> the absorption is indeed redshifted with about 80 nm. Besides, the absorption from 300 to 650 nm was interestingly induced as identified in Figure S6, Supporting Information, which is attributed to the introduction of conjugated TPE-T units and is rarely observed in reported CRs. Thus, the introduction of strong electron-donating TPE-T units indeed extends the absorption spectrum to cover both UV-vis and NIR regions. Remarkably, the absorption of CR-TPE-T can be further extended upon aggregation with the broad absorption spectrum from 300 to 1600 nm, which strongly facilitates the efficient sunlight harvesting. On the other hand, CR-TPE-T shows NIR emission at 965 nm in THF solution under 808 nm laser excitation (Figure 1c), showing much low fluorescence quantum yields with the value of 0.72%, which is well consistent with as-reported CRs.<sup>[17,18]</sup> Such emission of CR-TPE-T can be seriously quenched in the solid state with the negligible quantum yields of 0.01% (Figure 1c).

To get insight into the unique photophysical properties upon aggregation, the single crystal of CR-TPE-T was obtained in ethyl acetate (EA) under slow evaporation. Single-crystal X-ray diffraction analysis was carried out. As shown in Figure 1d and Figures S7 and S8 and Table S1, Supporting Information, three carbonyl bonds (C=O) uniformly disperse on five-membered ring in CR-TPE-T with the bond lengths of 1.242, 1.234, and 1.234 Å. Croconic core and thiophene units are coplanar and locked by intramolecular hydrogen bonds with distances of 2.470 and 2.493 Å, thus enhancing electron delocalization to extend the absorption in NIR region. Such unique coplanar thiophene-substituted croconic core can easily form strong intermolecular  $\pi$ - $\pi$  stacking with the distance of 3.430 Å as shown in Figure 1d, which could cause the serious emission quenching of CR-TPE-T.<sup>[25]</sup> Meanwhile, the intermolecular conjugation of CR-TPE-T can be enlarged by the  $\pi$ - $\pi$  stacking, which could further contribute to narrow the band gap to be 0.75 eV (Figure S9, Supporting Information) and broaden the absorption spectrum of CR-TPE-T.

Then, electron spin resonance (ESR) spectrum was used to characterize whether the radicals occur in CR-TPE-T. As shown in Figure 2a, it is interesting to observe ESR signals for CR-TPE-T with a  $g$  value of around 2.0043 in both solution and solid state. Compared to CR-TPE-T in solution, its ESR signal in the solid state is much higher (inset in Figure 2a). To further understand this, density functional theory (DFT) calculations were carried out at the  $\omega$ B97XD/6-31G\*\* level for CR-TPE-T in

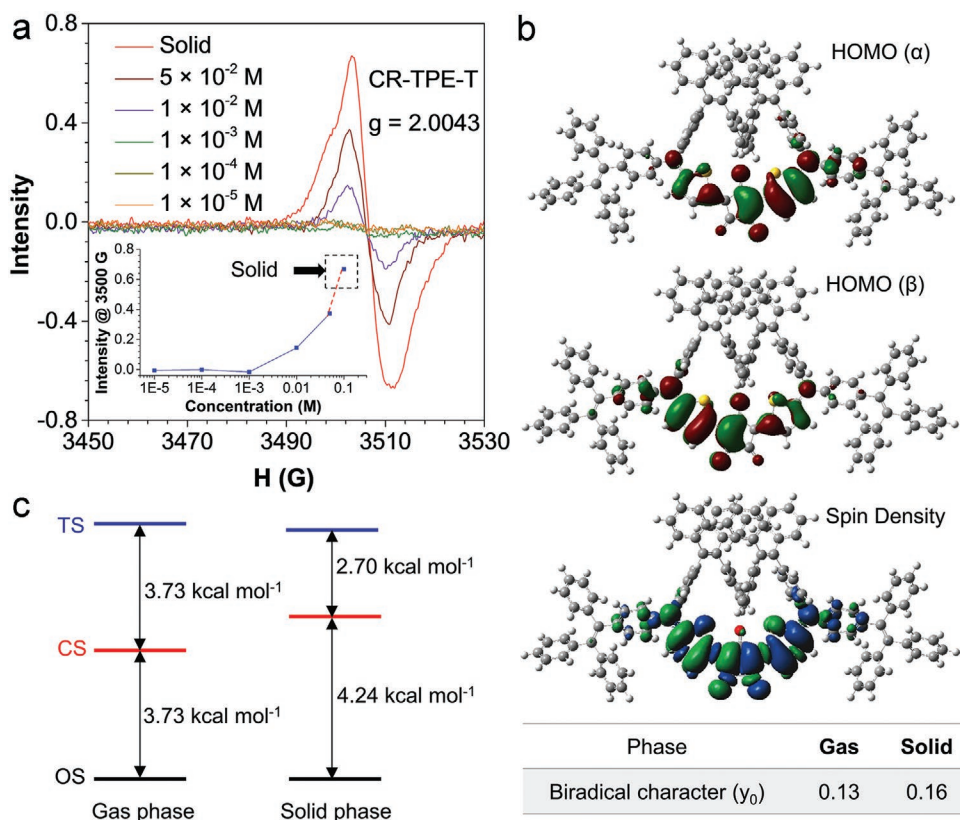


**Figure 2.** a) Electron spin resonance (ESR) spectra of CR-TPE-T in THF solution with different concentrations and solid. b) The calculated HOMOs for the  $\alpha$  and  $\beta$  electrons, the spin density distribution of the singlet biradical of CR-TPE-T, and the biradical character values ( $\gamma_0$ ) in the gas and solid phases. c) The energy levels of CR-TPE-T at the triplet state (TS), closed-shell singlet state (CS), and open-shell singlet state (OS).

the gas (representing the solution state) and solid phases (the computational details are given in Supporting Information). The calculated results indicate that CR-TPE-T in the both gas and solid phases exhibits singlet biradical property to some extent (Figure 2 and Figure S10, Supporting Information). In Figure 2b, the obtained highest occupied molecular orbital (HOMO) profiles of the  $\alpha$  and  $\beta$  spins of CR-TPE-T clearly depict a disjoint characteristic. More importantly, the separated spin densities (blue and green surfaces) are mainly distributed on the coplanar thiophene-substituted croconic core, indicating a large singlet biradical character for this molecule with different resonance structures (Figure S10, Supporting Information). The biradical character  $\gamma_0$ , representing the biradical natures between the closed-shell (CS) and pure open-shell (OS) diradical states (0–1),<sup>[23c]</sup> is further calculated in Figure 2b. The values of  $\gamma_0$  is increasing from 0.13 in the gas phase to 0.16 in the solid phase, which suggests that the biradical feature becomes stronger upon aggregation. Moreover, from the gas to solid phase, the energy gap between the CS and OS state is obviously upraised from 3.73 to 4.24 kcal mol<sup>-1</sup>, while the energy gap between the triplet state (TS) and OS state is decreased from 3.37 to 2.70 kcal mol<sup>-1</sup> in Figure 2c, which further bear out that CR-TPE-T in the solid state is closer to the ideal biradical state resulting in higher ESR signal. In addition, the biradical character is also calculated in THF solution and its value is determined to be 0.14, which is similar to the value of 0.13 in the gas phase and indicates the weak effect of solution on the biradical property.

Further, the photophysical properties of CR-TPE-T in CS and OS states were further evaluated by time-dependent DFT with  $\omega$ B97XD/6-31G\*\*. It is found that the spin of OS state is 1.799, which is much larger than 1.0 and close to 2.0, indicating radical nature. The first excitation energy of OS is 1.58 eV and it is higher than 1.69 eV of CS state. This causes the longer-wavelength NIR absorption in CR-TPE-T, agreeing well with the previous report that enhancing the biradical character of CRs can extend their NIR absorption.<sup>[20]</sup> Moreover, the smaller excitation energy always lead to fast nonradiative decay rate according to the energy-gap law. In addition, the oscillator strength ( $f$ ) of the lowest excited state is calculated to 1.1765 for CS-formed CR-TPE-T, while a negligible  $f$  of 0.0038 for OS-formed CR-TPE-T. This implies that the OS state would experience slower radiative decay process than that of CS state. Overall, the excited state energy of CR-TPE-T in the OS state tends to be consumed by nonradiative decay to generate heat. Thus, the higher biradical character of CR-TPE-T in the solid state largely boosts the emission quenching effect and enhances photothermal conversion by radical-promoted nonradiative decay.

Next, the photothermal property of CR-TPE-T was evaluated by rapidly recording the temperature changes under IR thermal camera. As shown in Figure 3a, 50 mg CR-TPE-T powder was irradiated by 808 nm laser with energy power of 0.8 W cm<sup>-2</sup>, the temperature increased dramatically to about 100 °C within 20 s, and then decreased quickly to room temperature within 10 s after removing laser, revealing a fast photothermal conversion process. The temperature changes during this process were carefully recorded as indicated in Figure 3b. With the higher power laser irradiation, the temperature raised up to be higher and the eventual temperature at the plateau was positively

related to the irradiation power of 808 nm laser (Figure S11, Supporting Information), indicating a superior photothermal behavior. Besides, the photothermal conversion efficiency for CR-TPE-T was estimated to be a high value of 72.7% (Figure S12, Supporting Information; details are shown in Supporting Information), which was a comparable value among those reported photothermal materials.<sup>[12,13]</sup> Notably, upon cycling of laser irradiation on and off for five times (Figure 3c) and long-time laser irradiation for 2 h (Figure S13a,c, Supporting Information), the photobleaching to photothermal behavior in terms of temperature loss for CR-TPE-T is not observed obviously, exhibiting excellent photostability superior to many traditional organic photothermal materials.

As abovementioned that CR-TPE-T is a high-performance and stable photothermal conversion material with a broad absorption spectrum from 300 to 1600 nm upon aggregation, it could be a promising candidate for capturing solar energy in solar-driving water evaporation. First, a type of commercial colorless and porous polyurethane (PU) foam with low thermal conductivity (pure PU, Figure 4a) was used as the supporting framework to establish an efficient interfacial evaporation system by floating on water.<sup>[8c]</sup> Then, CR-TPE-T was loaded inside this PU foam by impregnating pure PU foam in its dichloromethane (DCM) solution and drying under 80 °C, obtaining a brownish black PU foam (PU+CR-TPE-T, Figure 4a and Figure S14, Supporting Information). With insights into their structures by scanning electron microscopy (SEM), it is observed the rougher surface in PU+CR-TPE-T foam compared to pure PU foam, indicating the effective loading of CR-TPE-T in small aggregates that become larger and more as the loading amount of CR-TPE-T increased (Figures S15a and S16, Supporting Information). Such aggregated form will facilitate the effective sunlight harvesting for CR-TPE-T in PU+CR-TPE-T foam. As shown in Figure 4b and Figure S15b, Supporting Information, the absorption of PU+CR-TPE-T foam increased gradually when the loading amount of CR-TPE-T varies from 0 to 30 mg and remained almost unchanged with the further increase of loading, presenting excellent absorption properties with the full solar absorption spectrum covered nearly. On the other hand, the crisscrossed micropore structure inside the foam effectively enables water transporting and localizes the heat generated by CR-TPE-T to largely boost water evaporation.<sup>[5a,8c]</sup> As suggested in Figure S17, Supporting Information, PU+CR-TPE-T foam could get wetted uniformly within 60 s, indicative of the effective water transportation via the capillary condensation effect. And, the thermal conductivity of PU foam loaded without/with CR-TPE-T was measured to be 0.0341 and 0.0447 W m<sup>-1</sup> K<sup>-1</sup> for 23 °C, and 0.0447 and 0.0510 W m<sup>-1</sup> K<sup>-1</sup> for 43 °C, respectively (Figure S18, Supporting Information), exhibiting the low thermal conductivity to focus the thermal energy.

Further, the solar–thermal conversion of CR-TPE-T-loading PU foams were investigated by recording the temperature upon sunlight irradiation. As suggested in Figure S19a, Supporting Information, temperature on the surface of the PU+CR-TPE-T foams with different loading amounts of CR-TPE-T from 5 to 50 mg increases quickly up to an equilibrium within 200 s under 1 sun (1 kW m<sup>-2</sup>) irradiation in air, indicative of the fast response to solar light which contributes to the photothermal conversion. The more the loading amount of CR-TPE-T is, the

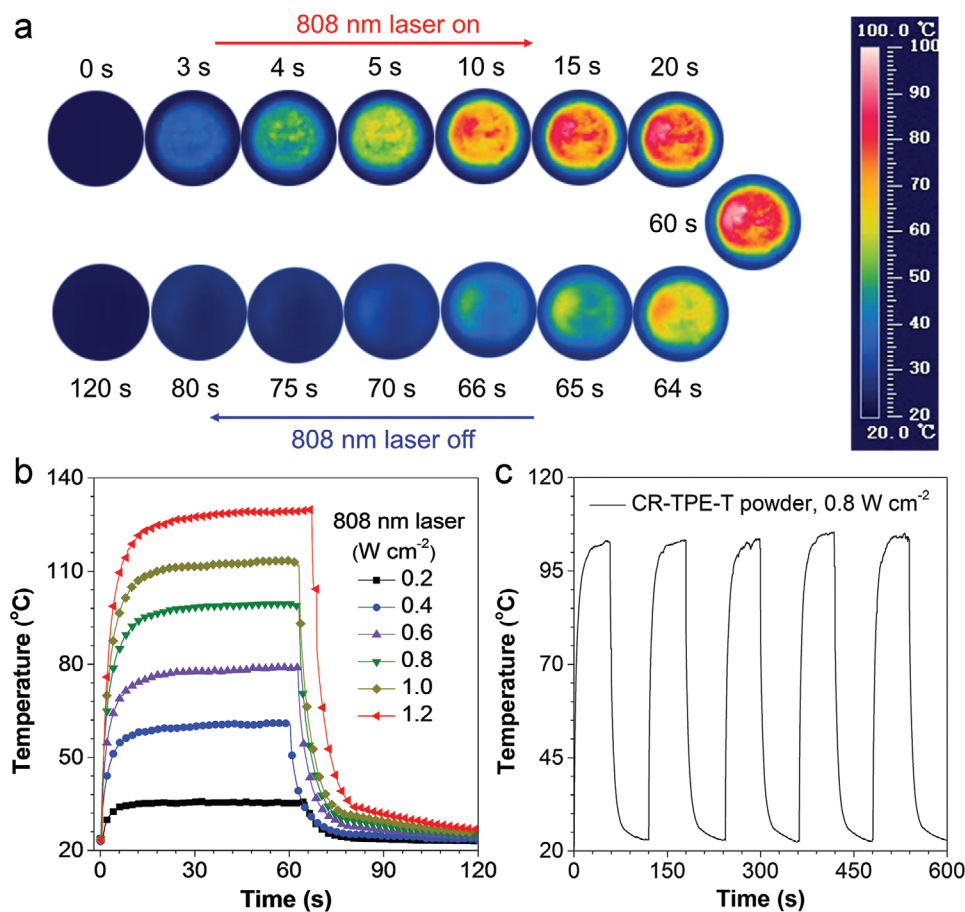


**Figure 3.** a) IR thermal images of CR-TPE-T powder (50 mg) under 808 nm laser irradiation ( $0.8 \text{ W cm}^{-2}$ ) and then turned off. b) Photothermal conversion behavior of CR-TPE-T powder under 808 nm laser irradiation at different laser powers (0.2, 0.4, 0.6, 0.8, 1.0, and  $1.2 \text{ W cm}^{-2}$ ). c) Anti-photobleaching property of CR-TPE-T powder during five cycles of heating-cooling processes.

higher the equilibrium temperature reaches. Among them, the equilibrium temperature of PU+CR-TPE-T foam with 30 mg of CR-TPE-T loading can reach to as high as  $77 \text{ }^\circ\text{C}$ , which is in sharp contrast to only  $30 \text{ }^\circ\text{C}$  for PU foam under the same condition (Figure 4c). As shown in the insets in Figure 4c, the IR thermal photos also exhibit a fascinating conversion capability from solar energy to heat under 1 sun irradiation in air by naked eye. Notably, such high temperature of PU-CR-TPE-T foam is attributed to the low thermal conductivity of PU and microporous heating localization. Moreover, the temperature stemmed from the solar-thermal conversion of CR-TPE-T-loading PU foam is almost not affected even after irradiation for 2 h, as indicated in Figure S13b,c, Supporting Information, revealing the excellent resistance to photobleaching the photostability.

Based on the integrated inspection, PU+CR-TPE-T foams with the efficient sunlight absorption and superior heating capability can be used as a heat generator for interfacial water evaporation system, with the basic design rationale illustrated in Figure 4d. Under the irradiation of sunlight, the water vapor was observed obviously on the top of the floated PU+CR-TPE-T foam, as shown in the insets in Figure 4e. The corresponding IR thermal photographs were taken by IR thermal camera and proved that the converted energy was indeed located in the

PU+CR-TPE-T foam on the interface between water and air, where the temperature of PU+CR-TPE-T foam is much higher than that of the bulk water maintained at room temperature of  $23 \text{ }^\circ\text{C}$ . Afterward, the temperature of foams on the surface of water was measured to further investigate the heat localization and solar-to-vapor conversion efficiency. As revealed in Figure 4e and Figure S19b, Supporting Information, the surface temperature of PU+CR-TPE-T foam floating on the water is remarkably higher than PU foam. The equilibrium temperature of the PU+CR-TPE-T foam loaded by 30 mg CR-TPE-T is  $43 \text{ }^\circ\text{C}$  after 1 sun illumination ( $1 \text{ kW m}^{-2}$ ) for 1 h, which is about  $10 \text{ }^\circ\text{C}$  higher than that of PU foam. Compared to the room temperature, about  $20 \text{ }^\circ\text{C}$  increment for PU+CR-TPE-T foam effectively facilitates the water evaporation according to the previous reports.<sup>[5]</sup>

To evaluate the efficiency of solar-driven water evaporation, the typical curves of time-dependent water mass change under solar irradiation (1 sun,  $1 \text{ kW m}^{-2}$ ) were measured under the simulated setup displayed in Figure S20, Supporting Information, with the data recorded real timely and in situ. As shown in Figure 4f and Figure S19c, Supporting Information, the evaporation of water by using PU+CR-TPE-T foam is greatly accelerated and the evaporation rate from the slope of time-dependent water mass change curves increases to be as high

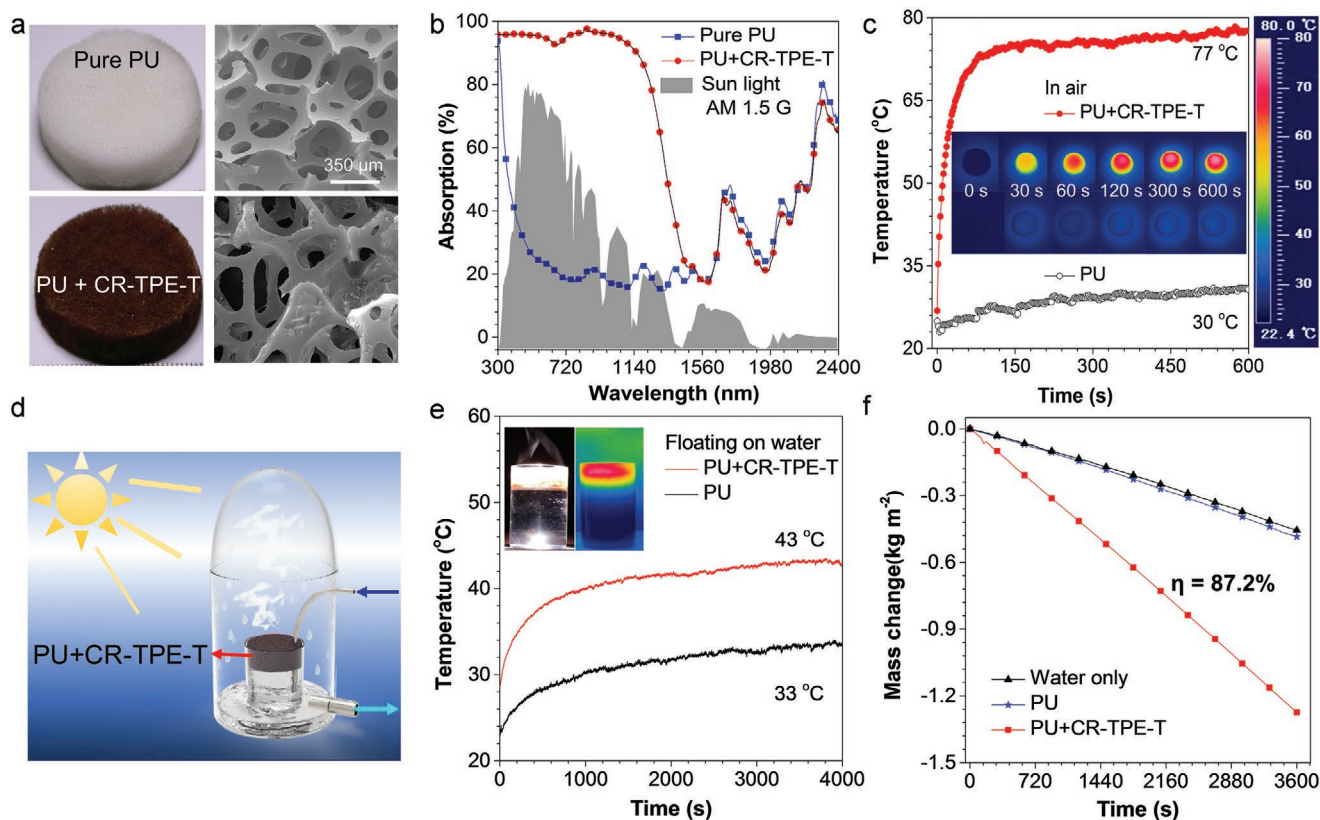


**Figure 4.** a) Digital photos and SEM images of pure (PU) and CR-TPE-T-loading PU (PU+CR-TPE-T) foams. b) The absorption of PU and PU+CR-TPE-T foams, and the solar spectral irradiance (gray). c) Photothermal conversion behavior of PU and PU+CR-TPE-T foams under 1 sunlight irradiation ( $1.0 \text{ kW cm}^{-2}$ ). Insets show IR thermal images of PU and PU+CR-TPE-T foams under 1 sunlight irradiation. d) The schematic illustration of solar-driven water evaporation. e) The temperature changes of PU and PU-CR-TPE-T foams floating on water against sunlight irradiation time. Insets show the photos under daylight and IR thermal camera upon 1 sunlight irradiation. f) Water evaporation curves without (water only) and with PU foam or PU-CR-TPE-T foam under simulated sunlight with an intensity of  $1 \text{ kW m}^{-2}$  (1 sun). The amount of CR-TPE-T used in preparing PU+CR-TPE-T foam is  $30 \text{ mg}$ . Room temperature is about  $23 \text{ }^\circ\text{C}$ .

as  $1.272 \text{ kg m}^{-2} \text{ h}^{-1}$ , compared to water only ( $0.445 \text{ kg m}^{-2} \text{ h}^{-1}$ ). While almost negligible increment was observed for PU foam ( $0.472 \text{ kg m}^{-2} \text{ h}^{-1}$ ), it evidently demonstrates the unique role of CR-TPE-T inside PU-CR-TPE-T foam on solar-driven water evaporation. Further, the efficiency of solar-driven water evaporation ( $\eta$ ) for PU+CR-TPE-T foam was calculated.<sup>[26]</sup> As suggested in Figure S19d, Supporting Information, the conversion efficiency of PU+CR-TPE-T increases with increasing of loading amount of CR-TPE-T from 0 to  $30 \text{ mg}$  and then remained with negligible change upon further increasing the loading amount of CR-TPE-T to  $50 \text{ mg}$ . The maximum  $\eta$  is calculated to be 87.2% when the loading amount of CR-TPE-T is  $30 \text{ mg}$  (details are shown in Supporting Information).

Moreover, we systematically evaluated the feasibility of employing CR-TPE-T for desalination of seawater. As shown in Figure S21, Supporting Information, real seawater sample was collected from the Yellow Sea, China, and subjected to the desalination experiment with CR-TPE-T. It was found that the concentrations of all the five primary ions ( $\text{Na}^+$ ,  $\text{Mg}^{2+}$ ,  $\text{Ca}^{2+}$ ,  $\text{K}^+$ , and  $\text{B}^{3+}$ ) originally present in the seawater were significantly reduced, which was lower than the values typically obtained through membrane-based method ( $10\text{--}500 \text{ ppm}$ ).<sup>[7a]</sup> Further, four representatives with different Na ions (0.8, 3.5, 4, and

10 wt%) were employed to study the impact of ion concentrations on the water evaporation rate and efficiency. Compared to the pure water (0 wt%), the water evaporation rate decreases from  $1.272$  to  $1.265$ ,  $1.208$ ,  $1.197$ , and  $1.191 \text{ kg m}^{-2} \text{ h}^{-1}$  with increasing ion concentrations, associated with the efficiency decrease from 87.2% to 87.1%, 83.2%, 82.5%, and 82.1%, respectively (Figure S22a, Supporting Information). Fortunately, the photostability of CR-TPE-T loaded PU foams is almost not influenced by the presence of ions as suggested in Figure 4e and Figure S22b, Supporting Information. On the other hand, the long-term stability was also examined by investigating the durability in real seawater (from the Yellow Sea, China) evaporation. As shown in Figure S23, Supporting Information, the desalination performance of PU+CR-TPE-T evaporation system under 1 sun illumination was maintained for more than 21 cycles with each cycle sustained for over 1 h. During the evaporation process, the CR-TPE-T-loaded PU foam retains an excellent photostability without obvious roll-off (Figure S24, Supporting Information).

In summary, a well-designed organic-small-molecule photothermal materials CR-TPE-T has been successfully obtained for solar-driven water evaporation. CR-TPE-T exhibits a broad absorption from 300 to  $1600 \text{ nm}$  in the solid state for efficient

sunlight harvesting. The radical signal is observed in CR-TPE-T by ESR spectrum, and it can be further enhanced upon aggregation. DFT calculation reveals the open-shell biradical nature and reasonably explains the redshift of the absorption promoted by the biradical. Then, the strong electron donor–acceptor coplanar skeleton in CR-TPE-T enables strong  $\pi$ – $\pi$  stacking analyzed by single-crystal X-ray diffraction, which largely extends the absorption in the solid state. On the other hand, the resultant small energy gap of 0.75 eV effectively boost nonradiative decay for generating heat according to the energy-gap law. Thus, CR-TPE-T exhibited superior and stable photothermal behaviors with a high efficiency larger than 72.7% under 808 nm laser irradiation. As concept of proof, a composite CR-TPE-T-loading PU foam was fabricated to establish an interfacial-heating evaporation system to obtain a comparable solar energy-to-vapor efficiency up to 87.2% and water evaporation rate of 1.272 kg m<sup>-2</sup> h<sup>-1</sup> under 1 sun irradiation, showing highly efficient solar-driven water evaporation. Considering the unique advantages of flexible, diverse structures, and tunable properties, organic-small-molecule photothermal materials would be extensively developed for effective solar energy conversion.

## Supporting Information

Supporting Information is available from the Wiley Online Library or from the author.

## Acknowledgements

G.C. and J.S. contributed equally to this work. This work was partially supported by the National Natural Science Foundation of China Grant (21702016, 21905015, and 21973099), Beijing National Laboratory for Molecular Sciences (BNLMS201813), the Fundamental Research Funds for the Central Universities (ZY1922), the Research Grant Council of Hong Kong (16305518, C6009-17G, and A-HKUST605/16), and the Innovation and Technology Commission (ITC-CNERC14SC01). X.G. acknowledges the theoretical calculation support from Prof. Z. S. and his student Q.S. B.Z.T. acknowledges the financial support from the National Science Foundation of China (21788102). The authors would like to thank Dr. Y. Li for the help of spectrum analysis. The authors also thank the Analysis and Test Center of Beijing University of Chemical Technology, and the Analytical Instrumentation Center, Peking University, Beijing 100871.

## Conflict of Interest

The authors declare no conflict of interest.

## Keywords

biradical character, croconium dyes, photothermal conversion, solar-driven water evaporation

Received: December 31, 2019

Revised: April 30, 2020

Published online: June 9, 2020

[1] a) S. U. M. Khan, M. Al-Shahry, W. B. Ingler Jr., *Science* **2002**, 297, 2243; b) M. Liu, M. B. Johnston, H. J. Snaith, *Nature* **2013**, 501,

- 395; c) F. Zhao, X. Zhou, Y. Shi, X. Qian, M. Alexander, X. Zhao, S. Mendez, R. Yang, L. Qu, G. Yu, *Nat. Nanotechnol.* **2018**, 13, 489.
- [2] N. S. Lewis, *Science* **2016**, 351, aad1920.
- [3] a) M. Gao, L. Zhu, C. K. Peh, G. W. Ho, *Energy Environ. Sci.* **2019**, 12, 841; b) L. Zhou, S. Zhuang, C. He, Y. Tan, Z. Wang, J. Zhu, *Nano Energy* **2017**, 32, 195.
- [4] a) L. Zhang, B. Tang, J. Wu, R. Li, P. Wang, *Adv. Mater.* **2015**, 27, 4889; b) Y. Liu, S. Yu, R. Feng, A. Bernard, Y. Liu, Y. Zhang, H. Duan, W. Shang, P. Tao, C. Song, T. Deng, *Adv. Mater.* **2015**, 27, 2768; c) H. Ghasemi, G. Ni, A. M. Marconnet, J. Loomis, S. Yerci, N. Miljkovic, G. Chen, *Nat. Commun.* **2014**, 5, 4449.
- [5] a) Y. Wang, C. Wang, X. Song, S. K. Megarajan, H. Jiang, *J. Mater. Chem. A* **2018**, 6, 963; b) P. Wang, *Environ. Sci.: Nano* **2018**, 5, 1078.
- [6] a) Y. Shi, R. Li, L. Shi, E. Ahmed, Y. Jin, P. Wang, *Adv. Sustainable Syst.* **2018**, 2, 1700145; b) M. Ye, J. Jia, Z. Wu, C. Qian, R. Chen, P. G. O'Brien, W. Sun, Y. Dong, G. A. Ozin, *Adv. Energy Mater.* **2017**, 7, 1601811.
- [7] a) L. Zhou, Y. Tan, J. Wang, W. Xu, Y. Yuan, W. Cai, S. Zhu, J. Zhu, *Nat. Photonics* **2016**, 10, 393; b) M. Chen, Y. Wu, W. Song, Y. Mo, X. Lin, Q. He, B. Guo, *Nanoscale* **2018**, 10, 6186; c) K. Bae, G. Kang, S. K. Cho, W. Park, K. Kim, W. J. Padilla, *Nat. Commun.* **2015**, 6, 10103.
- [8] a) J. H. Kim, S. H. Park, M. J. Lee, S. M. Lee, W. H. Lee, K. H. Lee, N. R. Kang, H. J. Jo, J. F. Kim, E. Drioli, Y. M. Lee, *Energy Environ. Sci.* **2016**, 9, 878; b) Y. Yang, R. Zhao, T. Zhang, K. Zhao, P. Xiao, Y. Ma, P. M. Ajayan, G. Shi, Y. Chen, *ACS Nano* **2018**, 12, 829; c) G. Wang, Y. Fu, A. Guo, T. Mei, J. Wang, J. Li, X. Wang, *Chem. Mater.* **2017**, 29, 5629.
- [9] a) L. Cui, P. Zhang, Y. Xiao, Y. Liang, H. Liang, Z. Cheng, L. Qu, *Adv. Mater.* **2018**, 30, 1706805; b) P. Zhang, J. Li, L. Lv, Y. Zhao, L. Qu, *ACS Nano* **2017**, 11, 5087; c) Q. Jiang, L. Tian, K. K. Liu, S. Tadepalli, R. Raliya, P. Biswas, R. R. Naik, S. Singamaneni, *Adv. Mater.* **2016**, 28, 9400.
- [10] a) Q. Chen, Z. Pei, Y. Xu, Z. Li, Y. Yang, Y. Wei, Y. Ji, *Chem. Sci.* **2018**, 9, 623; b) Q. Chen, X. Yu, Z. Pei, Y. Yang, Y. Wei, Y. Ji, *Chem. Sci.* **2017**, 8, 724.
- [11] R. Li, L. Zhang, L. Shi, P. Wang, *ACS Nano* **2017**, 11, 3752.
- [12] a) Z. Zhao, C. Chen, W. Wu, F. Wang, L. Du, X. Zhang, Y. Xiong, X. He, Y. Cai, R. T. K. Kwok, J. W. Y. Lam, X. Gao, P. Sun, D. L. Phillips, D. Ding, B. Z. Tang, *Nat. Commun.* **2019**, 10, 768; b) S. Liu, X. Zhou, H. Zhang, H. Ou, J. W. Y. Lam, Y. Liu, L. Shi, D. Ding, B. Z. Tang, *J. Am. Chem. Soc.* **2019**, 141, 5359.
- [13] a) H. S. Jung, P. Verwilst, A. Sharma, J. Shin, J. L. Sessler, J. S. Kim, *Chem. Soc. Rev.* **2018**, 47, 2280; b) C. Ji, W. Cheng, Q. Yuan, K. Müllen, M. Yin, *Acc. Chem. Res.* **2019**, 52, 2266; c) C. Liu, S. Zhang, J. Li, J. Wei, K. Müllen, M. Yin, *Angew. Chem., Int. Ed.* **2019**, 58, 1638.
- [14] a) R. Jiang, S. Cheng, L. Shao, Q. Ruan, J. Wang, *J. Phys. Chem. C* **2013**, 117, 8909; b) M. Camerin, G. Jori, L. D. Ciana, S. Fabbroni, S. Bonacchi, M. Montalti, L. Prodi, *Photochem. Photobiol. Sci.* **2009**, 8, 1422.
- [15] a) B. D. Richter, M. E. Kenney, W. E. Ford, M. A. J. Rodgers, *J. Am. Chem. Soc.* **1993**, 115, 8146; b) M. Camerin, S. Rello-Varona, A. Villanueva, M. A. J. Rodgers, G. Jori, *Lasers Surg. Med.* **2009**, 41, 665.
- [16] a) L. Cheng, W. He, H. Gong, C. Wang, Q. Chen, Z. Cheng, Z. Liu, *Adv. Funct. Mater.* **2013**, 23, 5893; b) C. S. Jin, J. F. Lovell, J. Chen, G. Zheng, *ACS Nano* **2013**, 7, 2541.
- [17] a) G. T. Spence, G. V. Hartland, B. D. Smith, *Chem. Sci.* **2013**, 4, 4240; b) X. Song, J. W. Foley, *Dyes Pigm.* **2008**, 78, 60.
- [18] a) L. Tang, F. Zhang, F. Yu, W. Sun, M. Song, X. Chen, X. Zhang, X. Sun, *Biomaterials* **2017**, 129, 28; b) S. Guha, G. K. Shaw, T. M. Mitcham, R. R. Bouchard, B. D. Smith, *Chem. Commun.* **2016**, 52, 120; c) G. T. Spence, S. S. Lo, C. Ke, H. Destecroix, A. P. Davis, G. V. Hartland, B. D. Smith, *Chem. - Eur. J.* **2014**, 20, 12628.

- [19] a) L. Liu, M. H. Liu, L. L. Deng, B. P. Lin, H. Yang, *J. Am. Chem. Soc.* **2017**, *139*, 11333; b) L.-X. Guo, M.-H. Liu, S. M. Sayed, B.-P. Lin, P. Keller, X.-Q. Zhang, Y. Sun, H. Yang, *Chem. Sci.* **2016**, *7*, 4400.
- [20] K. Srinivas, C. Prabhakar, C. L. Devi, K. Yesudas, K. Bhanuprakash, V. J. Rao, *J. Phys. Chem. A* **2007**, *111*, 3378.
- [21] a) X. C. Liu, P. Cai, Z. H. Chen, L. J. Zhang, X. F. Zhang, J. M. Sun, H. T. Wang, J. W. Chen, J. B. Peng, H. Z. Chen, Y. Cao, *Polymer* **2014**, *55*, 1707; b) X. Liu, B. He, C. L. Anderson, J. Kang, T. Chen, J. Chen, S. Feng, L. Zhang, M. A. Kolaczowski, S. J. Teat, M. A. Brady, C. Zhu, L. W. Wang, J. Chen, Y. Liu, *J. Am. Chem. Soc.* **2017**, *139*, 8355; c) B. Guo, Z. Sheng, D. Hu, A. Li, S. Xu, P. N. Manghnani, C. Liu, L. Guo, H. Zheng, B. Liu, *ACS Nano* **2017**, *11*, 10124.
- [22] a) Q. Song, Y. Jiao, Z. Wang, X. Zhang, *Small* **2016**, *12*, 24; b) Y. Jiao, K. Liu, G. Wang, Y. Wang, X. Zhang, *Chem. Sci.* **2015**, *6*, 3975; c) Y. Yang, P. He, Y. Wang, H. Bai, S. Wang, J.-F. Xu, X. Zhang, *Angew. Chem., Int. Ed.* **2017**, *56*, 16239; d) B. Tang, W.-L. Li, Y. Chang, B. Yuan, Y. Wu, M.-T. Zhang, J.-F. Xu, J. Li, X. Zhang, *Angew. Chem., Int. Ed.* **2019**, *58*, 15526; e) Y. Wang, W. Zhu, W. Du, X. Liu, X. Zhang, H. Dong, W. Hu, *Angew. Chem., Int. Ed.* **2018**, *57*, 3963.
- [23] a) Y. Li, L. Li, Y. Wu, Y. Li, *J. Phys. Chem. C* **2017**, *121*, 8579; b) Z. Zeng, S. Lee, M. Son, K. Fukuda, P. M. Burrezo, X. Zhu, Q. Qi, R. W. Li, J. T. L. Navarrete, J. Ding, J. Casado, M. Nakano, D. Kim, J. Wu, *J. Am. Chem. Soc.* **2015**, *137*, 8572; c) Y. Li, W.-K. Heng, B. S. Lee, N. Aratani, J. Zafra, N. Bao, R. Lee, Y. M. Sung, Z. Sun, K.-W. Huang, R. D. Webster, J. T. L. Navarrete, D. Kim, A. Osuka, J. Casado, J. Ding, J. Wu, *J. Am. Chem. Soc.* **2012**, *134*, 14913.
- [24] a) X. Hu, W. Xu, L. Zhou, Y. Tan, Y. Wang, S. Zhu, J. Zhu, *Adv. Mater.* **2017**, *29*, 1604031; b) Y. Ito, Y. Tanabe, J. Han, T. Fujita, K. Tanigaki, M. Chen, *Adv. Mater.* **2015**, *27*, 4302; c) L. Zhou, Y. Tan, D. Ji, B. Zhu, P. Zhang, J. Xu, Q. Gan, Z. Yu, J. Zhu, *Sci. Adv.* **2016**, *2*, e1501227; d) G. Ni, G. Li, S. V. Boriskina, H. Li, W. Yang, T. Zhang, G. Chen, *Nat. Energy* **2016**, *1*, 16126.
- [25] a) J. Mei, N. L. Leung, R. T. Kwok, J. W. Y. Lam, B. Z. Tang, *Chem. Rev.* **2015**, *115*, 11718; b) J. Yang, X. Zhen, B. Wang, X. Gao, Z. Ren, J. Wang, Y. Xie, J. Li, Q. Peng, K. Pu, Z. Li, *Nat. Commun.* **2018**, *9*, 840.
- [26] a) X. Li, J. Li, J. Lu, N. Xu, C. Chen, X. Min, B. Zhu, H. Li, L. Zhou, S. Zhu, T. Zhang, J. Zhu, *Joule* **2018**, *2*, 1331; b) C. Chen, Y. Kuang, L. Hu, *Joule* **2019**, *3*, 683; c) N. Xu, X. Hu, W. Xu, X. Li, L. Zhou, S. Zhu, J. Zhu, *Adv. Mater.* **2017**, *29*, 1606762; d) G. Chen, N. Zhang, N. Li, L. Yu, X. Xu, *Adv. Mater. Interfaces* **2020**, *7*, 1901715.